Energy and Buildings 86 (2015) 449–463

Contents lists available at ScienceDirect

Energy and Buildings

journal homepage: www.elsevier.com/locate/enbuild

The impact of exterior surface convective heat transfer coefficients on the building energy consumption in urban neighborhoods with different plan area densities

Jiying Liu[a,b], Mohammad Heidarinejad[c,d], Stefan Gracik[c], Jelena Srebric[b,c,d,*]

[a] School of Thermal Engineering, Shandong Jianzhu University, Jinan 250101, China
[b] Department of Architectural Engineering, The Pennsylvania State University, University Park, PA 16802, USA
[c] Department of Mechanical Engineering, The Pennsylvania State University, University Park, PA 16802, USA
[d] Department of Mechanical Engineering, University of Maryland, College Park, MD 20742, USA

ARTICLE INFO

Article history:
Received 5 June 2014
Received in revised form 23 October 2014
Accepted 25 October 2014
Available online 1 November 2014

Keywords:
Computational fluid dynamics
Convective heat transfer coefficient
Building energy consumption
EnergyPlus
Plan area density

ABSTRACT

In the urban micro-climate environment, the exterior surfaces' convective heat transfer coefficients (CHTCs) influence simulated building's energy consumption and exterior surface temperatures. This study first investigated the CHTCs at the external windward, leeward, and roof surfaces of a building located in an urban neighborhood with different plan area densities. New CHTC correlations were defined using the plan area density (λ_p), local velocity (U_{loc}), and temperature difference (ΔT), and then evaluated in the EnergyPlus simulation program. These new correlations and other commonly used correlations were employed to quantify the impact of CHTCs on the simulation results. The results show that the total cooling energy consumption increased by 4%, and the total heating energy consumption decreased by 1.3% when the plan area density increased from $\lambda_p = 0.04$ (almost isolated building) to $\lambda_p = 0.44$ (denser cities) due to the convective heat transfer from exterior building surfaces. With variable exterior surface CHTCs, the exterior surface temperature comparisons resulted in maximum temperature differences of 9.1 K and 3.6 K for the exterior south and north walls, respectively. Overall, this study quantified the impact of exterior surface CHTC correlations on the simulations results that directly impact the urban micro-climate.

1. Introduction

In the urban micro-climate environment, the convective heat transfer coefficients (CHTCs) at the exterior surfaces of a building are crucial parameters to accurately evaluate building thermal performance and associated building energy consumption [1,2]. Several studies have demonstrated that the simulated energy consumption can vary from 20% to 40% due to different choices of CHTC values for internal building surfaces [3–5]. Nevertheless, a critical literature review that focused on the exterior surface CHTC values showed that the simulated building energy consumption changed with the use of different CHTC correlations by up to 30% for isolated buildings and 80% for buildings in urban settings, indicating a fairly large influence of the CHTC values [6]. Furthermore, another study found the influence to be significantly less impactful with up to ±10% difference in the annual cooling energy consumption for different exterior CHTC correlations [7]. However, this study only took into account the ideal air load system and did not consider the shading and sheltering effects of different plan area densities (λ_p) on the CHTC correlations. Table 1 shows a summary of the maximum deviation of energy consumption, as well as the cooling and heating peak loads for the reviewed studies. Therefore, existing studies reported widely different values for the influence of the CHTC correlations on the building energy consumption, indicating a need to conduct a sensitivity analysis to further assess this influence.

Abbreviations: ACH, air change rate per hour; ASHRAE, American Society of Heating Refrigerating and Air-Conditioning Engineers; BCL, Building Component Library; BES, building energy simulation; BESTEST, building energy simulation test; CFD, computational fluid dynamics; CFL, Courant–Friedrichs–Levy; CHTC, convective heat transfer coefficient; CVRSME, coefficient of variation root square mean error; EPW, EnergyPlus weather; HVAC, heating ventilation and air conditioning; LRNM, low Reynolds number modeling; LES, large Eddy simulation; PISO, pressure-implicit with splitting of operators; PRESTO!, pressure staggering option; PTAC, packaged terminal air conditioner; RANS, Reynolds averaged Navier–Stokes; SST, shear stress transport; NMBE, normalized mean biased error; UQ, uncertainty quantification.

* Corresponding author at: Department of Mechanical Engineering, University of Maryland, College Park, MD 20742, USA. Tel.: +1 301 405 7276.
E-mail address: jsrebric@umd.edu (J. Srebric).

http://dx.doi.org/10.1016/j.enbuild.2014.10.062
0378-7788/

Nomenclature

A_d	lot area (m^2)
A_p	plan area of obstacles (m^2)
g	gravitational acceleration (m/s^2)
Gr	Grashof number
h_c	convective heat transfer coefficient ($W/(m^2\,K)$)
H	cubic height (m)
k	turbulent kinetic energy (m^2/s^2)
L	characteristic length (m)
q_{conv}	convective heat flux (W/m^2)
Re	Reynolds number
Ri	Richardson number
T	temperature (°C)
T_{bulk}	bulk temperature (°C)
T_{in}	inlet temperature (°C)
T_p	time period (s)
T_{surf}	surface temperature (°C)
u^*	friction velocity (m/s)
U_{10}	velocity at the height of 10 m (m/s)
U_{loc}	local velocity (m/s)
U_{met}	velocity in the meteorological station (m/s)
U_{ref}	velocity at the reference height (m/s)
y^+	dimensionless wall (normal) distance
z	height above the ground (m)
z_0	aerodynamics roughness length (m)
z_{met}	height of meteorological station (m)

Greek symbols

α	wind speed profile exponent
α_{met}	wind speed profile exponent at the meteorological station
β	thermal expansion coefficient (0.0035)
δ	boundary layer thickness (m)
δ_{met}	boundary layer thickness at the meteorological station (m)
ε	turbulent dissipation rates (m^2/s^3)
κ	von Karman constant (0.4)
λ_p	plan area density
Δ	difference

In recent years, many numerical simulations have been carried out in order to obtain better predictions of the CHTC at the external surfaces of buildings [2,8–10]. Moreover, there are a few studies that coupled building energy simulations (BES) and computational fluid dynamics (CFD) to provide more accurate estimates of CHTC values and building energy consumption [11,12]. Among these numerical studies, Reynolds-Averaged Navier–Stokes (RANS) equations with near wall modeling of Low Reynolds Number modeling (LRNM) and Large Eddy Simulation (LES) are two commonly used methods to predict CHTCs. Unfortunately, the two-equation turbulence models are not capable of resolving all complex features of the flow field around bluff bodies [13–18]. LES has been established as a more accurate tool for numerical computations of unsteady flows with complex flow structures in wind engineering applications [19], such as separation flows and flows around bluff bodies. Previous studies established that LES simulations with the Smagorinsky–Lily subgrid model provide more accurate results for CHTC in an array of cubes when compared to CHTC results from steady RANS including the realizable k–ε and the shear stress transport (SST) k–ω turbulence models [2]. In summary, outdoor airflow simulations using CFD can provide CHTC correlations for BES to improve the accuracy of the results, especially the LES method [20].

Several recent CFD studies resulted in different correlations that have been implemented in the EnergyPlus program [21]. However, these studies did not take into account the effect of buoyancy on CHTCs, which has since been proven to affect the CHTC [20]. The buoyant flows are mainly caused by the heat exchange between the outdoor airflow and building surfaces affected by the solar radiation [22]. Correspondingly, the sun shading from neighboring buildings could decrease the heat gain of building surfaces and surface temperatures, and will be an important parameter when evaluating the CHTC values and energy consumption [23]. In addition, the wind plays a significant role in the CHTC correlations, and the wind intensity, as well as direction, can also be strongly impacted by the building's surroundings [2]. In an urban environment, a building's surroundings could create a sheltering effect that can reduce local wind speeds. Alternatively, the building's surroundings could create urban canyons that increase local wind speeds. Therefore, an assessment of the local wind conditions for CHTC correlations is important for their accuracy. In summary, exterior surface CHTCs influence the results of simulated building energy consumption. It is important to quantify the influence of different CHTC correlations in the energy consumption results, considering the sun shading effect and wind sheltering effect.

In this paper, CFD simulations based on LES with the Smagorinsky-Lily subgrid model are first carried out to predict the CHTCs in a simplified urban area with different plan area densities. The calculated CHTC values are then used to define new surface-averaged CHTC correlations as a function of bulk wind speed (U_{10}), plan area density ($\lambda_p = A_p/A_d$ [24]), and temperature difference (ΔT) for windward, leeward, and top building surfaces. Where A_p and A_d are the lot area and plan area of obstacles, respectively, in the definition of the plan area density, representing the projected built area viewed from above to the total area in consideration. These correlations are implemented and compared with existing exterior surface CHTC correlations in EnergyPlus program to investigate the energy consumption considering different plan area densities, as well as the sun shading effect and wind sheltering effect. The overall goal of this study is to quantify the importance of the exterior CHTC correlations for simulation results of building energy consumption.

2. Methodology

This study was conducted in two phases: first investigate the CHTC values for different urban environments defined by their urban densities, and then quantify the impact of different CHTC values on the building energy consumption. Therefore, the two modeling approaches include: (1) CFD simulations for predicting CHTCs in urban areas, and (2) BES modeling for predicting energy

Table 1
Maximum deviations of energy consumption and cooling/heating peak loads.

Location of the building	Peak load		Energy consumption		Software	Building type	Literature
	Cooling	Heating	Cooling	Heating			
Basel, Switzerland	Up to 4%[a]	–	Up to 80% and 10%[a]	–	TRNSYS	Street canyon and Cubical building[a]	Allegrini et al. [20]
Brussels, Belgium	6%	–	30%	14%	ESP-r	Isolated building (10 m × 10 m × 10 m)	Mirsadeghi et al. [6]
Philadelphia, USA	5.3%	2.5%	10.1%	4.2%	EnergyPlus	Isolated building (10 m × 10 m × 10 m)	Liu et al. [7]

[a] The deviation for isolated building is specified calculated by author.

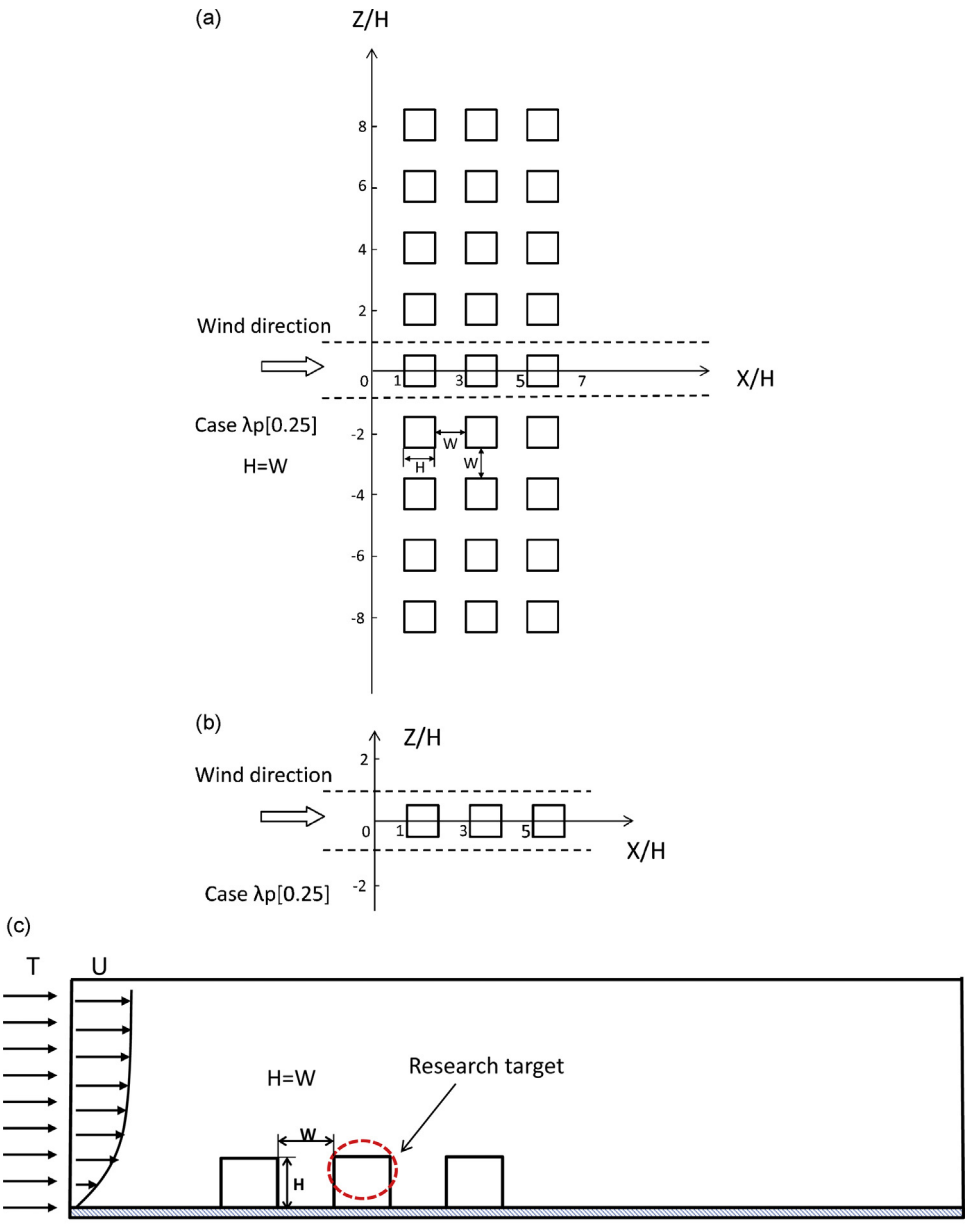

Fig. 1. Descriptions of the simplification process for computational model in Case λ_p [0.25]. (a) Whole distribution for entire models in horizontal plan, (b) intermediate simplified model in horizontal plan, and (c) final model in vertical cross section.

consumption based on different CHTC correlations. The investigation specifically focuses on the regular arrays of buildings immersed in a non-buoyant and buoyant boundary layer. This setup uses available measured data previously used for validation of flow field/CHTCs, and also it can be relatively easily characterized by the plan area density [2].

2.1. CHTC for regular arrays of buildings

To investigate surface heat transfer coefficients in different urban environments, a regular array of cubic buildings (H = 10 m), consisting of 3 rows, is modeled as shown in Fig. 1(a). This study focused on four different plan area densities (λ_p = 0.04, 0.11, 0.25, and 0.44) that result in different flow regimes, and used them for CHTCs analysis. Relative to the building array, the origin location is 1H upstream of the first building in the streamwise × direction at the ground level in the vertical y direction, and in the center of the middle building row in the spanwise z direction. The analysis case studies are named for different plan area densities with Case λ_p[0.04], Case λ_p[0.11], Case λ_p[0.25] and Case λ_p[0.44].

In this study, the CFD simulations were conducted using the control volume method with Ansys Fluent 12.0 [25], and validated with the wind tunnel experimental data provided by Meinders et al. [26]. LES with Smagorinsky–Lily subgrid model was compared with above data, as well as the realizable k–ε and the shear stress transport k–ω turbulence models. The results showed that both two-equation models underpredicted CHTC values compared to LES results. Moreover, the previous validation study also demonstrated that LES simulations with the Smagorinsky–Lily subgrid model can provide simulated CHTCs that are on average within 10% of the measured values [2]. This model was therefore used to provide CHTCs for new scenarios to investigate the influence of different flow regimes on the convective heat transfer. To reduce the simulation domain, this study assumed that the prevailing wind for the selected buildings is perpendicular to the building surfaces, enabling the assumption of symmetric boundary conditions.

Therefore, domain size for Case λ_p[0.25], the symmetry boundary conditions are applied at both sides of the simulation domain from $Z/H = -1$ to $Z/H = 1$, which is shown between the dotted lines in Fig. 1(b). The discussion section of this paper provides a brief summary of the potential impacts on the symmetry boundary conditions and CHTCs for the potential changes in the wind direction. In order to further reduce the requirement for the computational resource, the plane at the $Z/H = 0$ is employed to run two dimensional simulations. It should be noted that there are certain widths (=1 m) and grid numbers (=4) in the spanwise direction for the final models to enable the LES simulations. Fig. 1(c) shows the vertical cross-section of the computational domain for Case λ_p[0.25].

According to the recommendations from previous studies, a distance of 5H between the inflow boundary and the first building is required, and 15H between the outlet boundary and the last building of the domain is recommended [27]. In addition, the domain features a distance of 10H between the top boundary of the domain and the closest top surface of a building in order to keep the blockage ratio within 9.1% of the simulation domain's cross section. In this study, the top surface of the domain is represented by a symmetry plane. The ground surface of the domain is an adiabatic no-slip boundary with zero roughness. At the outlet boundary, outflow with zero-gradient is imposed in order to generate a fully developed flow. All the external surfaces of buildings are assumed to be no-slip boundaries with zero roughness height and imposed constant temperatures of 25 °C, 30 °C and 35 °C, respectively. The selection of these three imposed constant building surface temperatures enabled this study to consider the relative significance of natural and forced convective heat transfer processes. Differences between the inlet temperature and the building surface temperatures, commonly known as the surface-to-air temperature difference, are selected based on recommendations in the literature [8,28] to represent three surface-to-air temperature differences. Not only does the surface-to-air temperature difference determine the relative significance of the convective heat transfer processes, but the inlet velocity is also an important factor. Existing studies showed that a choice of 5 m/s as an inlet velocity represents a critical velocity in the determination of natural and forced convection heat transfer processes [8]. Therefore, the surface-to-air temperature differences of 5 °C, 10 °C, 15 °C with inlet velocity of 5 m/s are selected in this study to consider relative significance of the natural and forced convective heat transfer processes in the assessment of CHTC correlations.

At the inlet of the computational domain, the logarithmic wind profile and the turbulence specification method, including turbulent kinetic energy (k) and the turbulent dissipation rates (ε), are given as follows [29–31]:

$$\frac{U(z)}{u^*} = \frac{1}{\kappa}\ln\left(\frac{z+z_0}{z_0}\right) \quad (1)$$

$$k = \frac{u^{*2}}{0.3} \quad (2)$$

$$\varepsilon = \frac{u^{*3}}{\kappa(z+z_0)} \quad (3)$$

where κ is the von Karman constant ($\kappa = 0.4$), u^* is the friction velocity, and z_0 (=0.1 m) is the roughness length. The uniform temperature of 20 °C is specified as the inlet boundary condition. In order to present different thermal convection condition, Richardson number (Ri) is used as follows:

$$Ri = \frac{g\beta\Delta T L}{U_{ref}^2} \quad (4)$$

where g (=9.81 m/s^2) is the gravitational acceleration, β (=0.0035) is the thermal expansion coefficient, ΔT (K) is the temperature difference between inlet temperature (constant $T_{in} = 20$ °C) wall temperature, L (=10 m, same as the building height, H) is characteristic length, and U_{ref} (same as the velocity at the height of 10 m, U_{10}) is the bulk velocity. In this study, the Richardson number ranges from 0.03 to 80.05 based on different U_{10} and ΔT. Table 2 presents the detailed Richardson (Ri) number based on different bulk velocities (U_{10}) and temperature differences (ΔT).

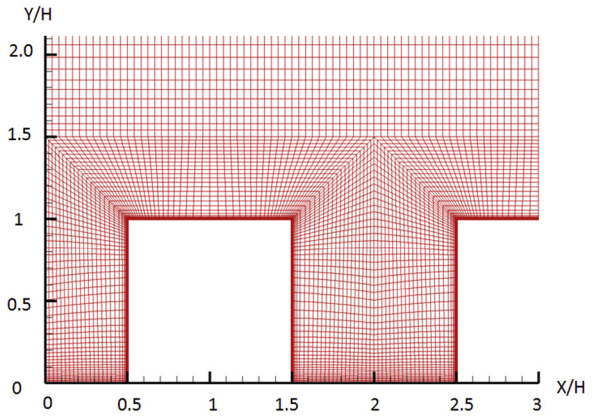

Fig. 2. The vertical cross-section of the computational grid distribution around one of the buildings.

A structured grid is employed in the entire computational domain, in which a small y^+ value ($y^+ \approx 1$) is required for wall-adjacent cells. To refine the grid close to the buildings, the maximum number of cells (48,520) is utilized for Case λ_p[0.04]. Fig. 2 shows the vertical cross-section of the computational grid distribution around one of the buildings. It should be noted that the grid independency evaluation is also carried out by changing grid numbers in the local computational zone around a building in all three directions [2]. For example, three different grid distributions including coarse grid, Δ_1: $40 \times 29 \times 40$, medium grid, Δ_2: $48 \times 35 \times 48$, and fine grid, Δ_3: $58 \times 42 \times 58$ for Case λ_p[0.25] with $U_{10} = 5$ m/s were compared. The results showed that the grid distribution of $48 \times 35 \times 48$ (H × W × L) was taken as the acceptable grid for independent flow field simulations around buildings. In the end, this grid distribution resulted in the averaged cell size changing from approximately 0.15 m × 0.15 m × 0.25 m (length × width × height) for Case λ_p[0.44] to $0.30 \times 0.30 \times 0.25$ for Case λ_p[0.04] for the wake region between two buildings.

In the LES simulations, the pressure was interpolated by a PRESTO! scheme [32]. The spatial discretization for the momentum and energy equations use the bounded central difference and second-order upwind scheme, respectively. Furthermore, the PISO scheme [33] was imposed for the pressure-velocity coupling method with the Skewness–Neighbor coupling. The time-dependent terms were interpolated by the implicit second-order interpolation scheme. The time step is set to $\Delta t = 0.01$ s for the Case λ_p[0.25] with $U_{10} = 5$ m/s, which ensures that Courant–Friedrichs–Levy (CFL) number (CFL = $u\Delta t/\Delta x$, where u is the local velocity magnitude and Δx is the local grid size), is always smaller than the CFL number in most of the grid points, with a maximal value of 2.0 in the region of high velocity around cube edges. The time periods 5 T_p ($T_p = L/U_{10}$, where L is the domain size) and 10 T_p are used to remove the influence of the initial condition, and provide the time-averaged data. Correspondingly, the time steps for all other cases range from 0.0075s to 0.05 s, due to the use of different U_{10} for different cases. Finally, according to the previous studies with instantaneous velocities [34–36], the time dependent boundary condition for inlet is imposed by means of a vortex method with 190 vortices.

Table 2
Richardson number based on different reference velocity (U_{10}), and temperature difference (ΔT).

U_{10} (m/s)	ΔT (K)	Ri (–)	U_{10} (m/s)	ΔT (K)	Ri (–)	U_{10} (m/s)	ΔT (K)	Ri (–)	U_{10} (m/s)	ΔT (K)	Ri (–)
	5	26.68		5	6.67		5	2.96		5	1.67
0.25	10	53.37	0.50	10	13.34	0.75	10	5.93	1.00	10	3.34
	15	80.05		15	20.01		15	8.89		15	5.00
	5	0.76		5	0.19		5	0.07		5	0.03
1.50	10	1.52	3.00	10	0.37	5.00	10	0.13	7.00	10	0.07
	15	2.28		15	0.56		15	0.20		15	0.10

2.2. Energy consumption for urban areas

EnergyPlus was applied as the BES program to perform the simulations. The basic test building (BESTEST Case 600 [37]) was a three story cubic building (10 m × 10 m × 10 m) with a single zone per floor, no interior partitions, and 15m^2 of windows on the south exposure as shown in Fig. 3(a). In order to investigate the shading effect of neighboring buildings, models with four different plan area densities (λ_p = 0.04, 0.11, 0.25, and 0.44) were utilized to predict the energy consumption based on different exterior surface CHTC correlations. Fig. 3(b) shows the view of the building models for an urban area with λ_p = 0.25.

This study used three different construction sets for the BESTEST Case 600, including (1) Pre-1980, (2) Post-1980 and (3) ASHRAE 189.1-2009 [37–39], representing buildings with different construction materials. Cooling and heating temperature set-points were 24 °C and 20 °C, respectively. All of the simulated buildings had a constant infiltration rate of 0.5 air change rate per hour (ACH) for each building floor. This is an assumption that has implication for the accuracy of simulation results, but the infiltration rate influence on the results is outside of the scope of this study that focuses on the convective heat transfer at the external building surfaces. A complementary study has investigated the influence of infiltration rate assumptions and calculation methodologies on the accuracy of energy simulation results [40]. Table 3 summarized the simulation setup in the energy model, including the occupant density, lighting level densities, and equipment power densities [39,41]. The service hot water was also provided with up to 3.17e−6 m^3/s (3 gallons/h). Philadelphia was selected as the primary location for this study; in addition, four different cities in the U.S. were selected including Miami, Phoenix, San Francisco, and Chicago, which represented different climatic conditions from very hot and humid to cool and humid climates as suggested in the literatures [42,43]. A Packaged Terminal Air Conditioner (PTAC) system was used to model the energy consumption with a default small office schedule from the Building Component Library (BCL) [44].

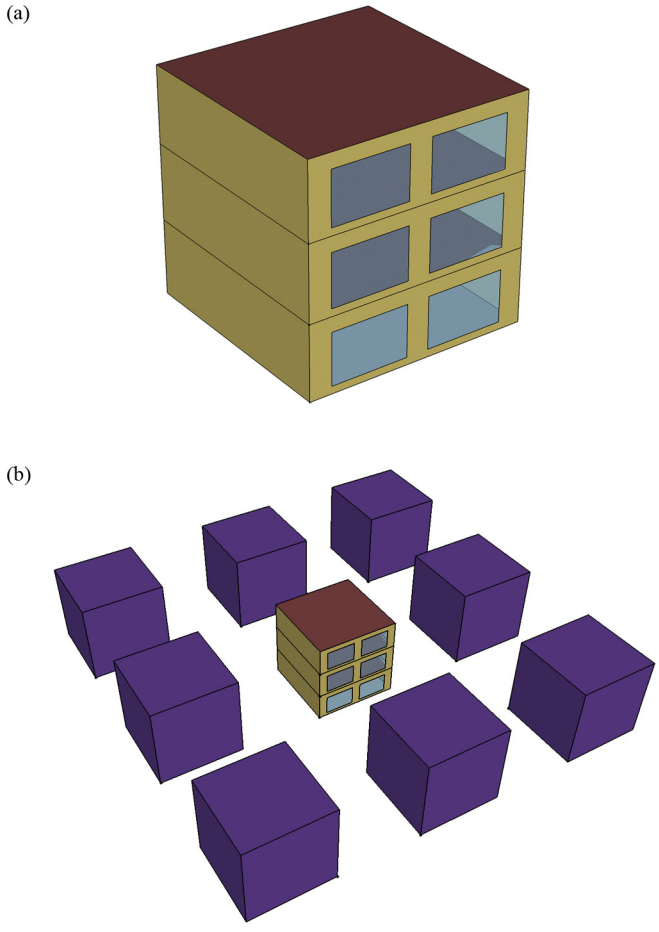

Fig. 3. The view of building models for isolated building (a) and an urban area with λ_p = 0.25 (b).

In the EnergyPlus program, there are over ten different exterior surface CHTC correlations. This study provides the list and simple descriptions for every exterior surface CHTC correlation as shown in Table 4, while the detailed explanations for the correlations can be found in the EnergyPlus Engineering Reference [21]. It is important to note that the default correlation used in EnergyPlus program is DOE-2, and there are a total of five commonly used correlations, including DOE-2, Simple Combined, TARP, MoWiTT, and Adaptive Convective Algorithm. Because the Adaptive Convection Algorithm can have its individual correlation selection, such as TARPWindward and ClearRoof for forced convection as well as ASHRAEVerticalWall for natural convection, this study chose five different options to compare the energy consumption based on different CHTC correlations. Note that the natural convection options in the Adaptive Convection Algorithm were constant and specified as ASHRAEVerticalWall for natural convection vertical correlation, and WaltonStableHorizontalOrTit for natural convection stable horizontal correlation. In addition, NusseltJurges, Mcadams, Mitchell, and Emmel correlations were modeled for every building surface, which did not take into account buoyancy effect. Finally, the additional exterior surface CHTC correlations, developed in the first phase of this study and implemented into EnergyPlus, were used to account for the urban plan density.

Table 3
Simulation setup in the energy model [39,41].

Load definitions	Value in IP (SI)
Occupants	0.005 people/ft^2 (0.05328 people/m^2)
Lighting	1 W/ft^2 (10.763910 W/m^2) Fraction radiant: 0.42 Fraction visible: 0.18
Electric equipment	1 W/ft^2 (10.763910 W/m^2) Fraction radiant: 0.3
Service hot water	3 gal/h (0.000003166667 m^3/s)
Heating set-point	20 °C
Cooling set-point	24 °C
Infiltration rate	0.5 Air change rate per hour (ACH)

Table 4
Exterior surface convection heat transfer coefficient correlations in EnergyPlus.

Correlations name	Description	Note
DOE-2[a]	$\sqrt{[aU_{\mathrm{loc}}^{b}]^2 + [c\lvert\Delta T\rvert^{1/3}]^2}$	Windward: $a=3.26$, $b=0.89$ Leeward: $a=3.55$, $b=0.617$ For $\Delta T<0$, $c = 9.42/(7.283 - \lvert\cos\Sigma\rvert)$ For $\Delta T>0$, $c = 1.81/(1.382 + \lvert\cos\Sigma\rvert)$
SimpleCombined	$D + EU_{\mathrm{loc}} + FU_{\mathrm{loc}}^2$	For rough brick, roughness coefficient $D=12.49$, $E=4.065$, $F=0.028$
TARP	$2.537W_f R_f \frac{PU_{\mathrm{loc}}}{A} + c\lvert\Delta T\rvert^{1/3}$	Windward: $W_f=1.0$, Leeward: $W_f=0.5$ For rough brick, roughness index $R_f=1.67$ Vertical surface, $c=1.31$, for others: When $\Delta T<0$, $c=9.42/(7.283-\lvert\cos\Sigma\rvert)$ When $\Delta T>0$, $c=1.81/(1.382+\lvert\cos\Sigma\rvert)$
MoWiTT	$\sqrt{[aU_{\mathrm{loc}}^{b}]^2 + [c\lvert\Delta T\rvert^{1/3}]^2}$	Windward: $a=3.26$, $b=0.89$, $c=0.84$ Leeward: $a=3.55$, $b=0.617$, $c=0.84$
Adaptive_default[b]	$Blocken_{\mathrm{Windward}} + Emmel_{\mathrm{Vertical}} + Clear_{\mathrm{Roof}}$	
Adaptive_TARP	$TARP_{\mathrm{Windward}} + TARP_{\mathrm{Leeward}} + Clear_{\mathrm{Roof}}$	
Adaptive_MoWiTT	$MoWiTT_{\mathrm{Windward}} + MoWiTT_{\mathrm{Leeward}} + Clear_{\mathrm{Roof}}$	Windward: $a=2.38$, $b=0.89$, $c=0.84$ Leeward: $a=2.86$, $b=0.617$, $c=0.84$
Adaptive_DOE2	$DOE2_{\mathrm{Windward}} + DOE2_{\mathrm{Leeward}} + DOE2_{\mathrm{Roof}}$	
Adaptive_Emmel	$Emmel_{\mathrm{Vertical}} + Emmel_{\mathrm{Vertical}} + Emmel_{\mathrm{Roof}}$	
Adaptive_Blocken	$Blocken_{\mathrm{Vertical}} + Emmel_{\mathrm{Vertical}} + Emmel_{\mathrm{Roof}}$	
NusseltJurges	$5.8 + 3.94U_{\mathrm{loc}}$	
Mcadams	$5.7 + 3.8U_{\mathrm{loc}}$	
Mitchell	$8.6U_{\mathrm{loc}}^{0.6}/L^{0.4}$	L is the cube root of the building's total volume
Emmel_Vertical	$aU_{10\,\mathrm{m}}^{b}$	$\theta \le 22.5$ $a=5.15$, $b=0.81$ $22.5 < \theta \le 67.5$ $a=3.34$, $b=0.84$ $67.5 < \theta \le 112.5$ $a=4.78$, $b=0.71$ $112.5 < \theta \le 157.5$ $a=4.05$, $b=0.77$ $157.5 < \theta \le 180.0$ $a=3.54$, $b=0.76$
Emmel_Roof	$aU_{10\,\mathrm{m}}^{b}$	$\theta \le 22.5$ $a=5.11$, $b=0.78$ $22.5 < \theta \le 67.5$ $a=4.60$, $b=0.79$ $67.5 < \theta \le 90$ $a=3.67$, $b=0.85$
Blocken_Windward	$aU_{10\,\mathrm{m}}^{b}$	$\theta \le 11.25$ $a=4.6$, $b=0.89$ $11.25 < \theta \le 33.75$ $a=5.0$, $b=0.80$ $33.75 < \theta \le 56.25$ $a=4.6$, $b=0.84$ $56.25 < \theta \le 100.0$ $a=4.5$, $b=0.81$
Clear_Roof	$\eta \frac{k}{L_n} 0.15 Ra_{L_n}^{1/3} + \frac{k}{x} R_f 0.0296 Re_x^{4/5} Pr^{1/3}$	Due to content limitation, all the coefficients can be found in the reference [52].

[a] Default correlation used in EnergyPlus. Note that, the details for values (a, b, c, etc.) can be found in the EnergyPlus Engineering Reference [21].
[b] For the default adaptive correlations and any other adaptive correlations mentioned in this table, the default natural convection for ASHRAE vertical walls ($c\lvert\Delta T\rvert^{1/3}$) were used, as well as WaltonStableHorizontalOrTit correlation for stable horizontal roof.

Among these correlations, the majority of the velocity values were represented by the local wind speed. In the EnergyPlus, the wind speed measured at a meteorological station is extrapolated to other altitudes (called local wind speed, U_{loc}) with Eq. (5), according to the ASHRAE Handbook of Fundamentals [21,45]. This equation converts the meteorological wind speed from the EnergyPlus Weather (EPW) file to the local wind speed, accounting for the urban terrain type.

$$U_{\mathrm{loc}} = U_{\mathrm{met}} \left(\frac{\delta_{\mathrm{met}}}{z_{\mathrm{met}}}\right)^{\alpha_{\mathrm{met}}} \left(\frac{z}{\delta}\right)^{\alpha} \tag{5}$$

where the exponent α is the wind speed profile exponent at the site, and the exponent δ is the wind speed profile boundary layer thickness at the site. The default value for z_{met} for measuring wind speed is 10 m above ground (U_{met}). Note that the wind speed profile coefficients α, δ, α_{met}, and δ_{met} are variables that depend on the roughness characteristics of the surrounding terrain. The typical values of α range from 0.14 for flat and open country to 0.33 for towns and cities, while the values for δ range from 270 to 460 for above terrain types. Therefore, there is one coefficient connected by local wind speed and meteorological station due to different measurement height, since the MoWiTT weather station height is 10 m and the window-centroid height is assumed to be 2 m [46]. In this study, the surface-averaged CHTC correlations will be derived based on bulk velocity at the height of 10 m, therefore, the velocity at the height of 5 m was selected as the local velocity. A coefficient value of 0.852 was finally obtained in the present study to present the relation of local wind speed and meteorological wind speed [46]:

$$U_{\mathrm{loc}} = 0.852 U_{\mathrm{met}} \tag{6}$$

It should be noted that this local wind speed represents the relation with meteorological wind speed, instead of being one value at the representative height/distance to nearing roof/wall, including 0.13–3 m by the literature investigation [47].

3. Results

The CHTC values for different urban neighborhoods, defined by their urban densities, resulted in different building surface temperatures. Furthermore, the energy consumption is also affected by varying exterior surface CHTC correlations. The investigation of the building's energy consumption included the shading effect and wind sheltering effect of neighboring buildings with different plan area densities.

3.1. CHTC correlations for different plan area densities

The surface-averaged CHTC is the major target of the current research work, which is calculated in CFD by the following equation:

$$h_c = \frac{q_{conv}}{T_{surf} - T_{bulk}} \quad (6a)$$

where q_{conv} is the convective heat flux, T_{surf} is the surface temperature, and T_{bulk} is the bulk temperature. Fig. 4(a) and (b) display the surface-averaged CHTC distributions in the cases of $\lambda_p = 0.11$ and 0.25 for windward, leeward, and roof surfaces with different incoming velocities and temperature differences (ΔT), respectively. These figures effectively demonstrated the importance of focusing on convective heat transfer due to buoyancy effect. The buoyancy force cannot be neglected, in this investigation it is specified by the incoming wind velocity of $U_{10} < 1.5$ m/s so that the Richardson number becomes larger than 2. When the incoming wind velocity is below 1 m/s, the CHTCs are not dominated by the incoming velocity and remain at a constant level, which can be explained by the fact that buoyancy which includes convective heat transfer has a significant effect on the calculated CHTCs as shown in Fig. 4. In the case of a mixed convective heat transfer regime, affected by both wind and buoyancy ($0.1 < Ri < 10$), the calculated CHTC values were still significantly altered by the presence of buoyancy force, especially for windward surfaces and leeward surfaces. For the roof surfaces, the buoyancy effect shows a negligible effect on the calculated CHTCs because larger local Reynolds numbers close to the building roof result in smaller local Richardson numbers ($Ri = Gr/Re^2$, where Gr is the Grashof number). Note that the calculated CHTCs, in the case of $\lambda_p = 0.11$, are larger than those in cases of $\lambda_p = 0.25$, indicating that denser urban areas lead to decreased forced convection due to wind. In addition, a transition regime from the wake interference flow regime to the isolated roughness flow regime, which is characterized by a small vortex occurrence behind the upwind building, resulted in a distinguished change in the velocity direction observed in the center of the building arrays [2,48]. For the case of $\lambda_p = 0.11$, windward CHTCs are within the same range of values with roof CHTCs, but higher than the leeward CHTCs. However, for the case of $\lambda_p = 0.25$, roof CHTCs are higher than windward and leeward CHTCs, and windward CHTCs have different patterns compared to the case of $\lambda_p = 0.11$. This change in patterns from $\lambda_p = 0.11$ to $\lambda_p = 0.25$ for the windward CHTCs originates from the influence of the sheltering provided by the surrounding buildings to the building being investigated. In summary, in the present study accounts for the combined effect of wind and buoyancy convective heat transfer at external building surfaces, which is necessary, and will be examined in the following section in detail.

This study uses the plan area densities (λ_p), bulk velocities (U_{10}), and temperature differences (ΔT) to define new CHTC correlations expressed as follows:

$$h_c = \sqrt{[(a + b\lambda_p)U_{10}^c]^2 + (d\Delta T^e)^2} \quad (7)$$

where a, b, d and c, e are three coefficients and two exponents, respectively. In general, the exponent c represents the effect of forced convection ranging from 0.7 to 0.9, while exponent e represents the effect of the forced convection and keeps the constant 1/3 according to the existing correlations in the EnergyPlus. But in this study the derivation process focused on a good curve fit that does not initially specify the exponents, therefore the derived exponent values may be shifted from the above range. Table 5 shows the derived correlations for different λ_p, U_{10} and ΔT, where λ_p varies from 0.04 to 0.44 and the Reynolds number ranges from 1.8×10^5 to 5×10^6. The local velocities were also used to derive the exterior surface CHTC correlations. Table 6 shows the new improved correlations for different λ_p, U_{loc} and ΔT, where λ_p varies from 0.04 to 0.44 and the bulk Reynolds number ranges from 1.8×10^5 to 5×10^6.

Table 5
Convective heat transfer coefficients (h_c) correlations combining λ_p, U_{10}, and ΔT for arrays of buildings.

Surface	h_c for arrays of buildings
Windward	$h_c = \sqrt{[(2.94 - 4.34\lambda_p)U_{10}^{0.94}]^2 + [1.52\lvert\Delta T\rvert^{0.36}]^2}$ ($R = 0.94$)
Leeward	$h_c = \sqrt{[(0.99 + 0.72\lambda_p)U_{10}^{0.94}]^2 + [1.52\lvert\Delta T\rvert^{0.36}]^2}$ ($R = 0.93$)
Roof	$h_c = \sqrt{[(3.13 + 1.50\lambda_p)U_{10}^{0.84}]^2 + [1.55\lvert\Delta T\rvert^{0.36}]^2}$ ($R = 0.91$)

According to the simulation results in Tables 5 and 6, a decrease in λ_p results in the decrease of CHTCs for the leeward and roof surfaces. This influence of λ_p on the CHTCs is mainly confirmed by the weaker descending airflow behind the upstream buildings. For the windward surfaces, however, the CHTCs actually increase with the decrease in the plan area densities λ_p. This inverse relationship is attributed to the gradual development of a horseshoe vortex with the greater building array's widths [2]. Therefore, with the increase of the plan area densities, CHTCs increase in the leeward and roof surfaces while decreasing in the windward surfaces, by up to 5%, 11%, and 38%, respectively, with constant bulk velocity ($U_{10} = 1$ m) and temperature difference ($\Delta T = 10$ K).

3.2. Sensitivity analysis of CHTCs influence on building energy consumption for different climates and thermal insulation of buildings

In order to analyze the influence of CHTC correlations on building thermal loads and energy consumption under different specific simulation setup conditions, various climate scenario and thermal insulation of buildings were investigated. In addition, to quantify the difference in the simulation results, the deviations of annual heating and cooling energy consumption were provided. The default CHTC correlations were selected to be DOE-2 correlation for exterior building surfaces, then the deviation in sequence was calculated as Eq. (8). Note that these deviations were defined for the specific climate and insulation scenarios. For example, for Tables 7 and 8, the average cooling energy consumption is calculated as the average of $\text{Deviation}_{(|\text{Simple-DOE2}|)}$, $\text{Deviation}_{(|\text{TARP-DOE2}|)}$, $\text{Deviation}_{(|\text{MOWITT-DOE2}|)}$, and $\text{Deviation}_{(|\text{Adaptive-DOE2}|)}$. Table 9 illustrates an example for the average cooling energy consumption of the building with Pre-1980 construction sets.

$$\text{Deviation}_{(|\text{Target-DOE2}|)}(\%) = \frac{E_{\text{Target}} - E_{\text{DOE2}}}{E_{\text{DOE2}}} \quad (8)$$

Table 7 provides the summary of the deviation results for the cooling/heating loads and energy consumption using different building thermal insulation conditions. This table shows that with the use of better-insulation building materials, the effect of CHTC correlations becomes weaker. When the building materials for pre-1980 were used, the average deviation of cooling thermal loads and cooling energy consumption can reach 12.2% and 9.6%, respectively. However, when the building materials for ASHRAE

Table 6
Convective heat transfer coefficients (h_c) correlations combining λ_p, U_{loc}, and ΔT for arrays of buildings.

Surface	h_c for arrays of buildings
Windward	$h_c = \sqrt{[(3.39 - 5.03\lambda_p)U_{loc}^{0.94}]^2 + [1.52\lvert\Delta T\rvert^{0.36}]^2}$ ($R = 0.94$)
Leeward	$h_c = \sqrt{[(1.15 + 0.82\lambda_p)U_{loc}^{0.94}]^2 + [1.52\lvert\Delta T\rvert^{0.36}]^2}$ ($R = 0.93$)
Roof	$h_c = \sqrt{[(3.57 + 1.72\lambda_p)U_{loc}^{0.84}]^2 + [1.55\lvert\Delta T\rvert^{0.36}]^2}$ ($R = 0.91$)

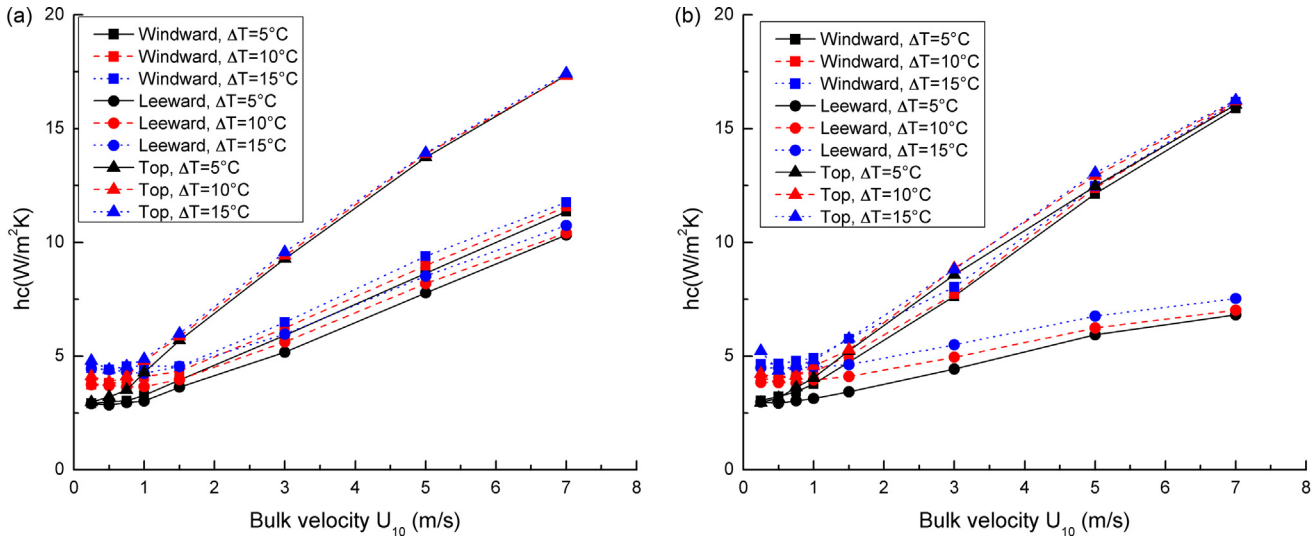

Fig. 4. The surface-averaged CHTC distributions in the cases of $\lambda_p = 0.11$ (a) and $\lambda_p = 0.25$ (b) for windward, leeward and roof surfaces with different incoming velocity and temperature difference (ΔT).

189.1-2009 were selected, the CHTC only affected the cooling thermal loads and cooling energy consumption with an average value of 3.0% and 2.3%, respectively. These results show that the thermal loads and associated energy consumption could be significantly reduced by improving the building thermal insulation. Because the well-insulating building materials have been required in the past decades, this study considers only insulation values meeting ASHRAE 189.1 2009 to analyze the impact of CHTC correlations.

Table 8 shows a summary of the deviation of cooling/heating loads and energy consumption for different climate scenarios. In general, when the heating loads are lower than the cooling loads in a specific climate, the deviations in the heating loads increase. Correspondingly, the deviations in cooling loads increase when the heating loads are higher. This phenomenon is also present for the building energy consumption. For example, Miami and Phoenix are located in the cooling dominated climate, so the heating loads/energy consumption were approximately only 1/40–1/100 of the cooling loads/energy consumption in these two cities. Therefore, the deviations for heating loads in Miami and Phoenix were larger than that in Philadelphia and Chicago, with the maximum value of up to 11.3%. Overall, from the hot climates to cold climates, the maximum (average) deviations for heating loads and heating energy consumption becomes smaller, approximately ranging from 11.3% (5.7%) to 5.3% (2.9%) and 7.5% (3.3) to 4.0% (2.3%), respectively. Furthermore, all the maximum and average deviations for

Table 7
Maximum deviations of cooling/heating load and energy consumption for different building thermal insulation levels.

	Heating load			Cooling load			Heating energy consumption			Cooling energy consumption		
	Max	Min	Ave	Max	Min	Ave	Max	Min	Ave	Max	Min	Ave
Pre-1980	9.8%	0.4%	3.7%	21.1%	7.1%	12.2%	12.1%	1.6%	5.6%	16.5%	6.0%	9.6%
Post-1980	7.4%	0.1%	2.8%	11.3%	2.3%	6.2%	6.9%	0.9%	3.1%	8.3%	1.0%	4.7%
ASHRAE 189.1-2009	6.0%	1.0%	3.0%	4.3%	0.9%	3.0%	4.5%	0.9%	2.4%	3.3%	0.5%	2.3%

Note: The Philadelphia weather condition was used in this case.

Table 8
Maximum deviations of cooling/heating load and energy consumption for different climate scenarios.

	Heating load			Cooling load			Heating energy consumption			Cooling energy consumption		
	Max	Min	Ave	Max	Min	Ave	Max	Min	Ave	Max	Min	Ave
Miami, FL	9.8%	0.9%	5.7%	4.5%	0.0%	3.1%	7.5%	0.9%	3.3%	3.7%	0.7%	2.5%
Phoenix, AZ	11.3%	0.5%	4.8%	3.1%	0.5%	2.3%	6.7%	0.5%	3.3%	2.6%	0.4%	1.7%
San Francisco, CA	8.5%	4.7%	5.9%	7.7%	2.3%	5.8%	6.6%	3.6%	4.5%	9.0%	3.5%	7.3%
Philadelphia, PA	5.9%	1.0%	3.0%	4.3%	0.9%	3.0%	4.5%	0.9%	2.4%	3.3%	0.5%	2.3%
Chicago, IL	5.3%	1.8%	2.9%	4.6%	1.0%	3.5%	4.0%	1.4%	2.3%	3.5%	0.5%	2.6%

Note: The ASHRAE 189.1-2009 building thermal insulation was used in the case.

Table 9
An example calculation of the deviation between the results for the target and default CHTC values.

	DOE-2	Simple	TARP	MoWiTT	Adaptive
Cooling consumption (J)	4.253×10^{10}	3.928×10^{10}	4.607×10^{10}	4.509×10^{10}	3.550×10^{10}
Absolute difference between the target CHTC and DOE-2 (%) specified in Eq. (8)	–	7.6	8.3	6.0[a]	16.5[a]
Average cooling energy consumption difference (%)	–	9.6			

[a] Maximum and minimum values are 16.5% and 6.0%, respectively.

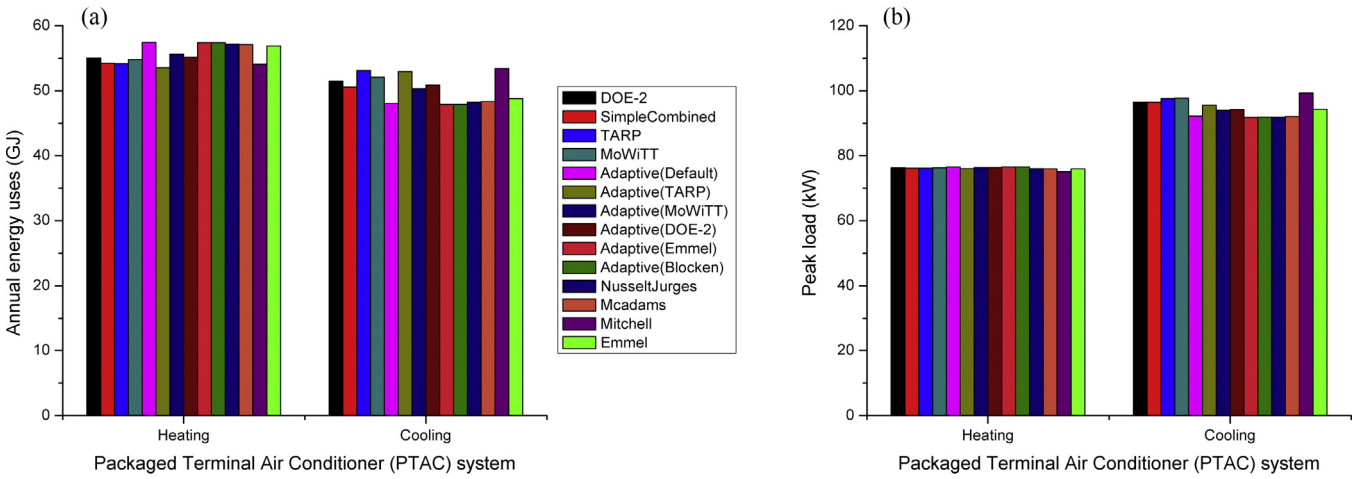

Fig. 5. Annual heating/cooling (a) energy uses and (b) peak loads with the use of different existing CHTC correlations.

cooling loads and cooling energy consumption showed relatively stable values ranging from 1.7% to 4.6%. However, in San Francisco, the deviations exhibited different trends, with the averaged deviation value for cooling loads and cooling energy consumption of up to 5.8% and 7.3%, respectively. Comparatively, cooling and heating energy consumptions are more sensitive to CHTC correlations in the San Francisco because this climate is relatively mild and requires less heating and cooling compared to the other climates [42].

In Table 8, a comparison between thermal loads and energy consumption showed that the deviations of thermal loads were slightly larger than that of energy consumption, with 2.4% largest average deviation for the building heating results using ASHRAE 189.1-2009 construction materials. This result indicates that the CHTC correlations have slightly larger effect on the thermal loads than energy consumption. In addition, Table 7 shows that the cooling loads at most had only 2.6% higher average variation than the heating consumption for the buildings with Pre-1980 and Post-1980 construction materials. Nevertheless, the difference between the average deviations in cooling loads and consumption is at most only 0.7% for the building with ASHRAE 189.1-2009 construction materials.

In summary, the results of the sensitivity analysis presented in Tables 8 and 9 for the buildings with different building construction materials and located in different climates suggest: (1) exterior CHTC models have slightly more influence on the cooling and heating loads than the cooling and heating energy consumption, (2) older buildings with lower thermal insulation levels are more susceptible to the choice of exterior CHTCs, (3) buildings located in hotter climate conditions may experience a higher variation in the heating loads and heating energy consumption than the cooling loads and cooling energy consumption compared to other climates.

3.3. *Effect of CHTC correlations in different plan area densities on energy consumption*

Fig. 5 shows peak thermal loads and annual energy consumption for a building located in Philadelphia, using the fourteen different CHTC correlations in EnergyPlus program. This figure indicates that exterior surface CHTCs have a more significant effect on the cooling energy consumption rather than the heating energy consumption. Specifically, the maximum deviations for cooling and heating energy consumptions were slightly small, with up to roughly ±7% and ±4%, respectively. In addition, the maximum deviations of the heating peak loads due to the change of exterior surface CHTCs is remarkably smaller than that of the cooling peak loads, with up to roughly ±5% and ±2%, respectively. Also, Cooling energy consumption was more dependent on the outdoor thermal environment than heating energy consumption, which agrees with prior research [39,41]. Therefore, it can be concluded that the accurate utilization of exterior surface CHTCs does not play a significant role in eliminating the discrepancy of estimation on heating energy consumption. Admittedly, the comparisons demonstrated that the existing CHTCs provide sufficiently accurate energy consumptions, especially when studying the effect of exterior surface CHTCs on the cooling energy consumption. In addition, the maximum deviation of cooling peak loads due to the change of exterior surface CHTCs is considerably larger than that of heating peak loads as shown in Fig. 5(b).

The new derived correlations for the different plan area densities shown in Table 5 are implemented in the EnergyPlus. Fig. 6 shows the heating and cooling energy uses with the use of an improved CHTC correlation, compared to DOE-2 and MoWiTT correlations. The results show that although a decrease of up to 38% was observed for CHTC correlations with the increase of the plan area densities from $\lambda_p = 0.04$ to $\lambda_p = 0.44$, the differences of cooling and heating energy consumption appears slightly smaller, with maximum discrepancy of 4.0% and 1.3%, respectively. This phenomenon is similar to the results displayed in Table 6, which presents the exterior surface CHTC correlation with no significant

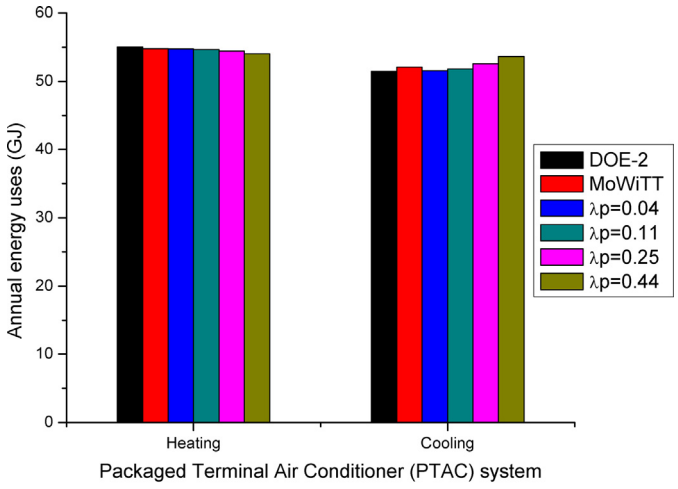

Fig. 6. Annual heating and cooling energy uses with the use of newly developed CHTC correlations.

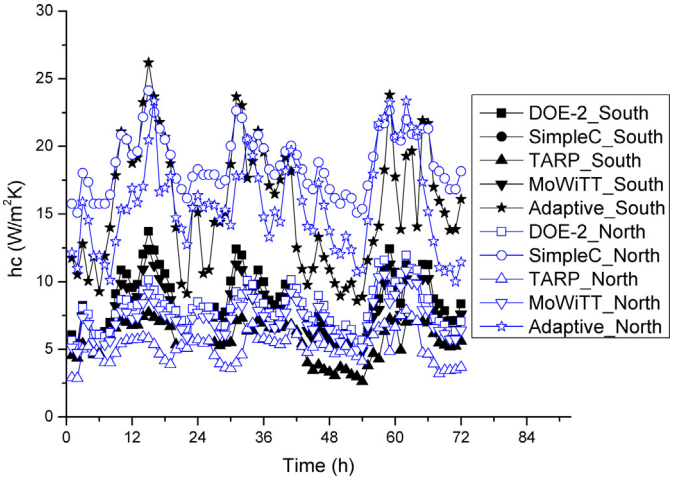

Fig. 7. The variation of commonly used exterior surface CHTCs in hot weather conditions (From July 7 to 9).

influence on the energy consumption. In summary, the impact of different exterior surface CHTC correlations on the building energy consumption is compared and quantified. In addition, the five commonly used exterior surface correlations were specifically taken into account to investigate the variation of surface CHTCs and surface temperatures.

3.4. Exterior surface CHTCs variation and its effect on building wall temperature

Based on the results above, the effect of exterior surface CHTCs on the cooling energy consumption is less significant when compared to the heating energy consumption. Therefore, this section only investigated the variation of commonly used exterior CHTCs in hot weather conditions. Fig. 7 shows the variations of exterior south and north surface CHTCs in hot weather conditions for 72 h from July 7 to July 9. The results show significant differences between the exterior south and north surface CHTCs, in which a variation of up to 300% is observed for CHTCs. Therefore, to accurately calculate CHTCs it is necessary to estimate surface exposure to strong winds and incoming solar raditaion.

Note that in Fig. 7 the SimpleCombined correlations overlapped, and had the same values for south and north walls. This is because the correlation oversimplified the expressions and only forced convection was considered without distinguishing between the windward or leeward surfaces shown in Table 4. For adaptive algorithms, very large CHTC values with up to 300% deviation of were observed compared to DOE-2, TARP, and MoWiTT correlations. This phenomenon is considering odd because after investigating the weather data, the maximum local velocity is only up to 4.4 m/s. Therefore, this study suggests using discretion when assigning the SimpleCombined and AdaptiveAlgorithm correlations. In addition, validation is highly recommended to ensure its accuracy. The results also showed that exterior surface CHTC values roughly range from 4 W/m^2 K to 12 W/m^2 K without taking into account Simple and Adaptive correlations.

This study also provided building wall temperature variations due to the use of different exterior surface CHTCs. Figs. 8 and 9 show the interior and exterior surface south/north temperature variations, resulting from different CHTCs in hot weather conditions from July 7 to July 9. The simulations first showed that exterior surface CHTCs do not affect interior surface temperatures when air conditioner is on. In another words, the well-insulated building wall acts as an effective thermal resistance, and does not significantly affect the inside surface heat balance equation. For the exterior surface tempeature, these comparisons showed that the maximum temperature differences are approximately 9.1 K and 3.6 K for the exterior south and north considering variable exterior surface CHTCs, respecitivly. This phenomena is due to the different shading effect from the adjacent buildings. Therefore, taking into account the incoming solar raditation is important for accurate calculations of the surface temperautre and corresponding energy consumption. The observed influence of the exterior sufrace temperatures due to the change of CHTCs has implications on the degradation of the building exterior construction materials.

Fig. 10(a) and (b) showed the changes in annual heating and cooling energy consumption due to the shading effect of neighboring buildings in different plan area densities. The simulation model for Case $\lambda_p = 0.25$ can be found in Fig. 3(b). Here, all the cases only considered the default DOE-2 correlation, and with a PTAC HVAC system. The results showed that there was an increase of up to a 32% for heating energy uses, and a decrease of up to 24% for cooling energy uses were observed, with the increase of the plan area densities from $\lambda_p = 0.0$ (isolated) to $\lambda_p = 0.44$ (denser

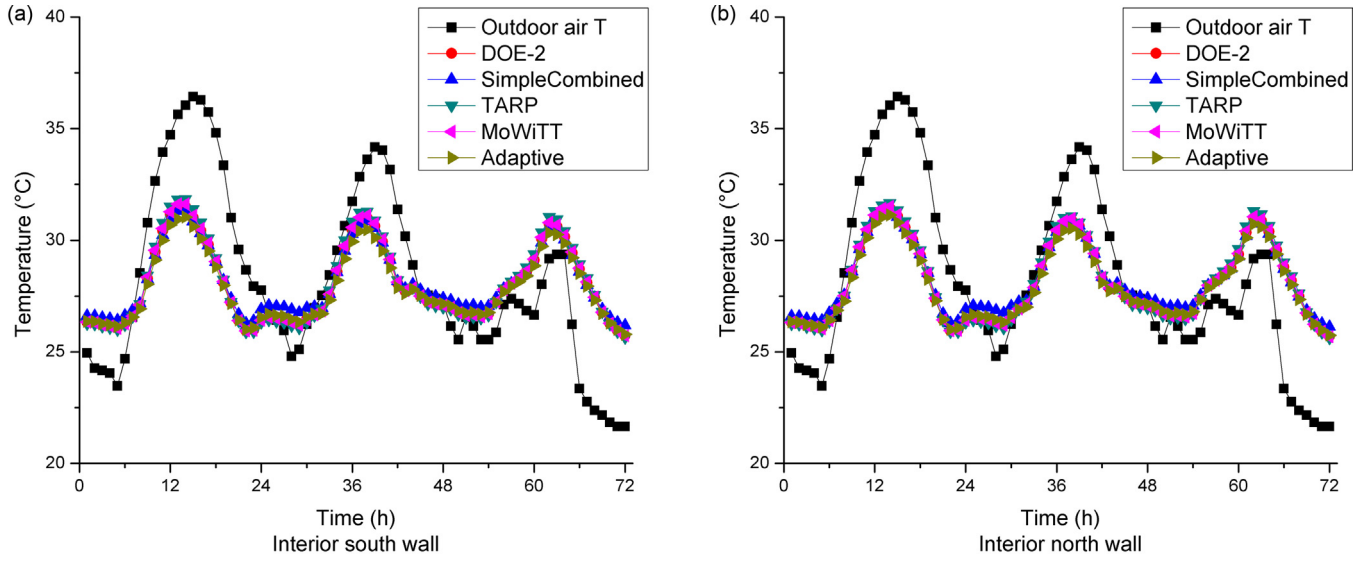

Fig. 8. The interior south wall (a) and north wall (b) temperature variation due to the use of commonly used CHTC correlations.

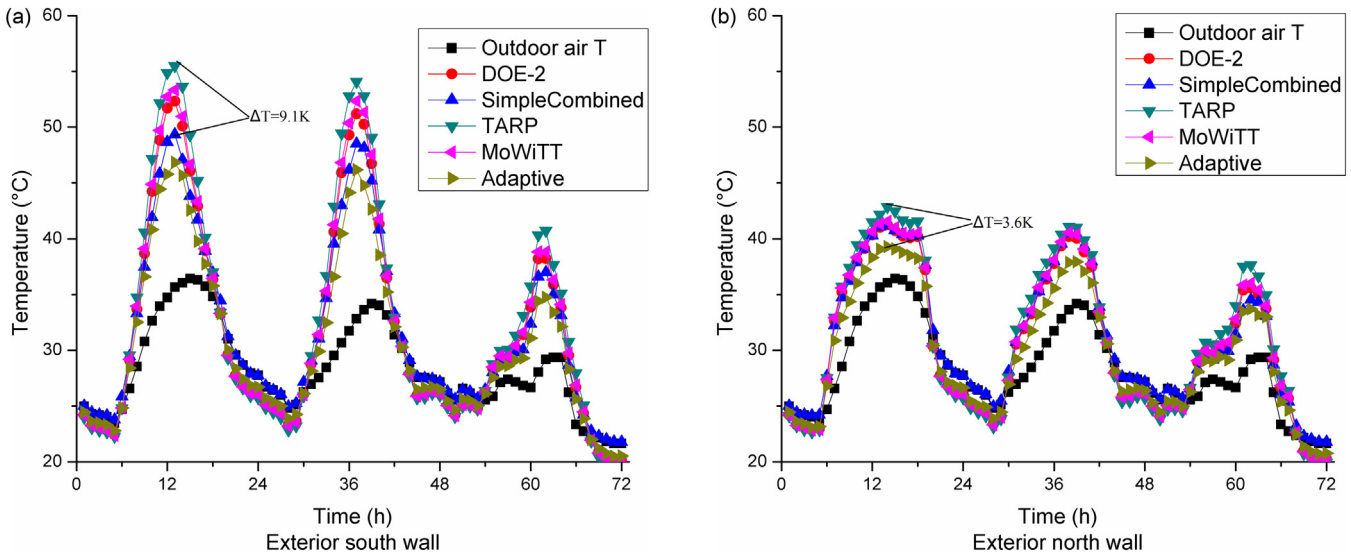

Fig. 9. The exterior south wall (a) and north wall (b) temperature variation due to the use of commonly used CHTC correlations.

cities). This discrepancy was very significant, due to the shading effect that caused a significant difference in surface temperatures. Therefore, the exterior surface temperatures are calculated by the external surface heat balance equation, which is often effected by the solar radiation in urban environment. Therefore, further studies will focus in detail on the effects of urban heat island on the enegy consumption.

3.5. *Wind sheltering effect of terrain type on energy consumption*

Although the significant effect of exterior surface CHTCs on energy consumption is not expected, this present study provides one comparison of wind sheltering effects on energy consumption by investigating the terrain type in the EnergyPlus program. As presented for the calculation of local wind speed, the default wind speed profile exponent (α) and wind speed profile boundary layer thickness (δ) at the simulation sites are 0.14 and 270 for flat and open surroundings, respectively. Considering the effect of terrain type, this study selected different options for α and δ, including 0.14 and 270, 0.22 and 270, 0.22 and 370, 0.33 and 370, and 0.33 and 460. Fig. 11 shows the annual cooling and heating energy uses with different terrain types due to the wind sheltering effect. The result shows that the heat energy consumption decreased up to 3.5%, and the cooling energy consumption increased up to 6.7%. Although this difference is slight, most of existing studies did not take into account the effect of this parameter, which only used the default setup of terrain type. This result also shows the necessity to measure local wind velocities, because the present EnergyPlus simulations utilized the local wind speed rather than bulk velocity at the meteorological station site. In fact, the local velocities change frequently around the building, resulting in relatively high uncertainties for the measured wind velocities. It is important to note that in this analysis the infiltration rate remains constant. This issue might be resolved by using the CFD simulation coupled with the BES method to provide a more accurate estimation of the local wind speed and airflow temperature, in addition to the exterior surface CHTCs in urban areas.

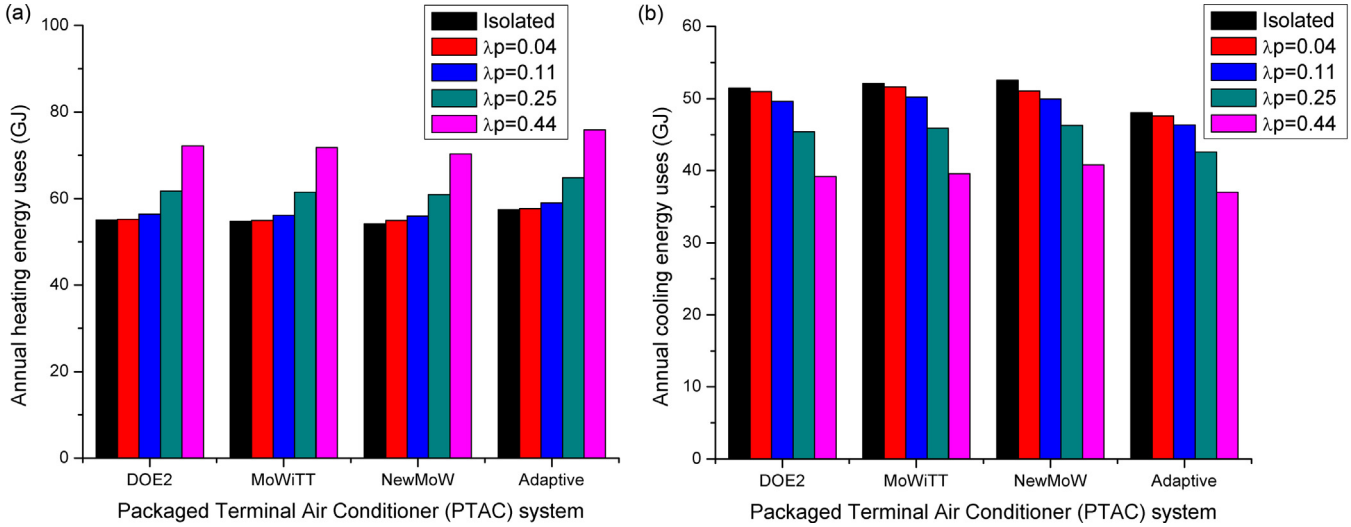

Fig. 10. Changes in the annual (a) heating and (b) cooling energy consumptions due to shading effect of neighboring buildings in different plan area densities (only default DOE-2 correlation is considered).

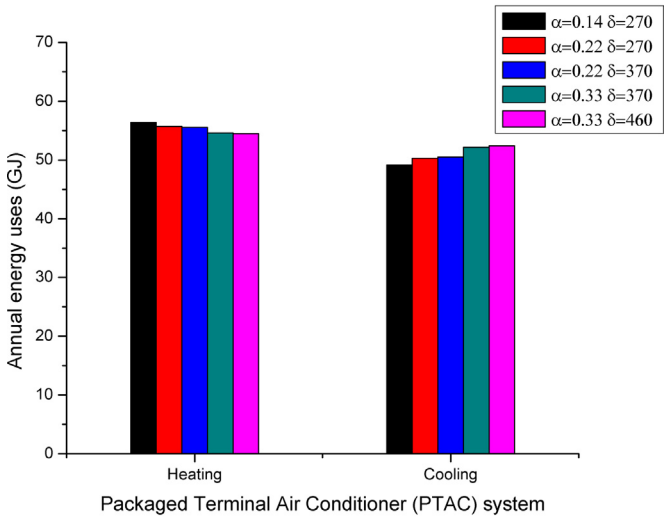

Fig. 11. The annual cooling and heating energy uses with different terrain types.

4. Discussion

This section provides discussion on the influence of the selection of the CHTCs on a calibrated energy model and the broader implications for the results of this study for urban neighborhoods with different configurations.

4.1. Implications on the calibrated energy models

To investigate the influence of the CHTCs on the accuracy of building energy simulations, this study examined the importance of using suitable CHTCs to calibrate an energy simulation model. Accuracy of building energy simulations highly depend on the accuracy of the inputs [49]. Therefore, the selection of CHTCs could render an uncalibrated energy model calibrated or a calibrated model uncalibrated. For the cases of Pre-1980, Post-1980, and ASHRAE 189.1, Table 10 provides a sensitivity analysis for the monthly heating and cooling energy consumptions with the selection of TARP and Adaptive CHTC models. Normalized Mean Biased Error (NMBE) and coefficient of variation root square mean error (CVRSME) are two metrics suggested by ASHRAE Guideline 14 to assess accuracy of a building energy model [50]. It is important to note that the original purpose of Guideline 14 was to evaluate accuracy of a calibrate model. This study benefited from the metrics developed in this guideline to explore the possibility of rendering an uncalibrated model to a calibrated model or vice versa. The results in Table 9, especially for the Pre-1980, indicate that the results of the CVRSME and NMBE are outside of the confidence interval recommended in ASHRAE Guideline 14 even with the existence of a metered energy data for the simulated case study. This confirms the influence of the CHTC models on the accuracy of building energy simulations is significant when a calibrated energy model is needed.

4.2. Broader implications

This section briefly discusses the influence of urban neighborhood configurations, including spacing and height of buildings, wind speed direction, and building shape, on the calculation of the CHTCs. These discussions provide a broader range of applicability for the cases when the urban neighborhood does not meet the requirements specified in this study.

This study considered buildings of similar size and shape to determine characteristics of the CHTCs based on airflow patterns. The benefit of this approach is to develop a replicable study with potentially generalizable results. For example, the set of cubes selected in this study can represent buildings located in urban neighborhoods where buildings are within the same height. Washington DC is an example of urban neighborhoods where buildings have mostly similar heights. However, urban neighborhoods are often comprised of a mixture of low-rise and high-rise buildings. For cities such as Los Angles, a more realistic approach would take into account variation of building shapes and different configuration of the urban neighborhood. In general, the cities in the U.S. have more variability in the height compared to the European cities This study considered buildings of similar size and shape to determine characteristics of the CHTCs based on airflow patterns. The benefit of this approach is to develop a replicable study with potentially generalizable results. For example, the set of cubes selected in this study can represent buildings located in urban neighborhoods where buildings are within the same height. Washington DC is an example of urban neighborhoods where buildings have mostly similar heights. However, urban neighborhoods are often comprised of a mixture of low-rise and high-rise buildings. For cities such as Los Angles, a more realistic approach would take into account variation of building shapes and different configuration of the urban neighborhood. In general, the cities in the U.S. have more variability in the height compared to the European cities [51], suggesting there is a higher potential to utilize the results of this study for the European cities. Urban neighborhoods comprised of only high-rise or only low-rise buildings correspond to the neighborhood layout in this study. For urban neighborhoods with a mixture of low-rise and high-rise buildings, if the building of interest is a high-rise building surrounded by low-rise buildings, there will be little influence on heating and cooling loads, as the low-rise buildings do not appreciably alter airflow patterns or provide shading for the building of interest. If the building of interest is a low-rise building surrounded by any high-rise buildings, then there are significant changes in airflow pattern and shading which depart significantly from what is considered in this study. Further consideration of characteristic dimensions, such as frontal area density, will require additional CFD analysis.

Existing studies showed that considerations of the wind direction depend on the location of the selected building or urban neighborhood. For locations where the variation of the wind direction during the day is not significant, there is no need to consider the effect of the wind direction on the CHTCs [28]. On one hand, a set of studies showed that the variation of the CHTCs become important when the wind direction changes [8,52,53]; on the other hand, there are studies that showed the variation of the CHTCs due to the changes in the wind direction is less significant [9]. Overall, based on the results of published studies, it is recommended to include a variation of 25% to include the effect of the wind direction in the Uncertainty Quantification (UQ) of the energy simulations [8]. This UQ assessment due to the impact of the wind direction could be added to the existing UQ studies for the influence of the CHTCs on the building energy simulation results [54]. The impacts of the wind direction on the CHTCs become more important when the building does not have a cubic shape. The difference between wind directions could be roughly up to 25% for the windward walls [8]; leeward walls and the roof are less sensitive to the variation of the wind direction [8].

For the selected urban neighborhood in this study, due to the symmetry of the urban neighborhood, absence of solar radiation, and consideration of uniform spacing between buildings, one can consider only 1/8 of the urban neighborhood to assess the impacts of wind direction on the urban neighborhood. This suggests an angle of incidence needs to be varied from 0 to 45°. This study recommends considering up to 25% variation in the UQ studies due to the changes of the wind direction. In general, EnergyPlus assumes the surface windward when the incidence angle normal to

Table 10
Comparison of CVRSME and NMBE between TARP and Adaptive models with the use ASHRAE Guideline 14 metrics.

	Pre-1980		Post-1980		ASHRAE 189.1	
	Heating consumption	Cooling consumption	Heating consumption	Cooling consumption	Heating consumption	Cooling consumption
CVRSME	22.5%	37.3%	14.4%	19.6%	10.2%	7.6%
NMBE	16.0%	−32.5%	10.3%	−15.6%	7.2%	−6.2%

Note that in the CVRSME and NMBE, y_i is simulated result using the Adaptive CHTC model and $\hat{y}$ is the simulated result using the TARP model in the analyses based on ASHRAE Guideline 14. In addition, acceptable energy model needs to have CVRSEM and NMBE less than 15% and 5%, respectively, for the monthly analyses.

the wall and the incoming wind direction is less than ±90, meaning EnergyPlus uses the CHTCs developed for the windward walls; otherwise, the wall is considered as the leeward wall and the leeward CHTCs are used.

In addition, a slight change in the wind direction has influence on the mesh generation and results of the CFD simulations. When the flow is not perpendicular to the building surfaces, the errors usually originate from the discretization schemes [55]. A common method uses prevailing wind direction and magnitude as a constant value [2]. An extended version of this approach performs the simulations for a set of prevailing wind directions and magnitudes to assess the effectiveness of changes in wind directions and magnitude [9,56]. The third approach utilizes a stochastic model and cylindrical coordinates to consider variations of the wind direction and magnitude during the generation of mesh and potential impacts on the simulation results [57]. In general, the wind direction influences the airflow pattern around the buildings, causing impacts on the simulated CHTCs. This study assumes that the prevailing wind for the selected buildings is perpendicular to the building surfaces, enabling assumptions of the symmetric boundary conditions and grid independency tests for the CFD results. This assumption is valid for locations where the wind rose from the meteorological weather data suggests the prevailing wind direction remain relatively unchanged.

For the urban neighborhoods comprised of rectangles, ellipses, circles, and hexagons, there is also a need to consider a range of variations in the UQ of the energy simulations. One important parameter in the determination of the heat transfer rates in addition to the characteristics of the airflow pattern is the characteristics length of the buildings used in the calculation of the Nusselt Number. When the rectangular, cubical, elliptical, and circular buildings have the same characteristics length, buildings with streamlined shapes have lower heat transfer rates and CHTCs, due to delayed separation of the air flow around the streamlined buildings compared to the less streamlined buildings [58]. For example, in general, it is expected that the rectangles, hexagons with the edge in front of the incoming flow, and the ellipses perpendicular to the incoming flow have a higher CHTCs compared to the results of this study. For the shapes with more streamlined shapes, such as the circles and ellipses, when they are placed parallel to the airflow direction, the CHTC values are lower than the results of this study. Since the separation happens in higher angles for the streamlined shapes, more surfaces are in direct connection with the flow. Overall, due to the complex nature of the airflow around the buildings, there is a need for future studies to quantify the influence of the building shapes on the CHTCs for buildings located in an urban neighborhood.

Determination of the plan area urban density and spacing of the buildings for an actual neighborhood is another important parameter that distinguishes the results of this study and an actual urban neighborhood. This study assumes buildings are located with a uniform spacing. For the urban neighborhoods, when the buildings are located in a semi-regular or irregular spacing, there is a need to provide recommendations for calculations of urban density. In general, with reasonable simplifications, it is possible to determine plan area density for most of the urban neighborhoods. Burley [59] showed how an actual urban neighborhood for the Penn State's campus can be divided into seven different plan area densities. Moreover, Liu et al. [60] and Gracik [61] used one of the seven urban densities to consider an urban neighborhood with uniform spacing between the buildings. The procedure used in these three studies confirmed that a semi-regular urban neighborhood could be considered as a combination of regular and irregular neighborhoods. However, for irregular neighborhoods, buildings after the first row of the buildings only serve as roughness elements in the airflow simulations. Therefore, with a careful assessment of the roughness influenced by the sheltering buildings in the CFD simulation, it is possible to create customized CHTCs for any irregular neighborhoods. This effort of developing customized CHTCs requires substantial work to model an individual urban neighborhood in the CFD simulations and calculate customized CHTCs for the building energy simulations.

5. Conclusions

This study used LES with the Smagorinsky–Lily model to define exterior surface CHTC correlations with different plan area densities (λp), local wind velocities (U_{loc}), and temperature differences (ΔT). These density-dependent CHTC correlations found in this investigation were implemented in the EnergyPlus program to study their effect on the energy consumption and building surface temperatures in urban settings. The energy consumption sensitivity analysis used the resulting density-dependent CHTCs, as well as five commonly used correlations with three HVAC systems, for a total of eighteen case studies. In order to analyze the sensitivity of energy simulation results, this study used five representative climate scenarios and three different building insulation levels to understand the importance of CHTCs for modeling of buildings. Miami, Phoenix, San Francisco, Philadelphia, and Chicago were selected to represent cooling dominated, heating dominated, and mild climates. In general, when the heating loads are one order of magnitude lower than the cooling loads, the deviations in the loads calculated by different CHTCs were more significant. This suggested that the deviations for heating loads in Miami and Phoenix were larger than that in Philadelphia and Chicago. The deviations for Miami, Phoenix, Philadelphia, and Chicago were 9.8%, 11.3%, 5.9%, and 5.3%, respectively. Cooling loads in cities except in San Francisco showed lower sensitivity (up to 4.6%) to the selection of the CHTCs, suggesting the selection of the CHTCs has more influence (up to 7.7%) in the mild climates. Pre-1980, post-1980, and ASHRAE 189.1 2009 were the three selected building insulations in this study to evaluate the influence of the building insulations. While for the pre-1980, the average deviation of the cooling loads can reach to 12.2%, for buildings with better insulations, including post-1980 and ASHRAE 189.1, the influence is only 6.2% and 3.0%, respectively.

For an urban neighborhood with plan area densities that range from $\lambda_p = 0.04$ (almost isolated building) to $\lambda_p = 0.44$ (denser cities), the results show that the differences in the total cooling and heating energy consumption were up to 4% and 1.3%, respectively. The exterior surface temperature comparisons showed that the maximum temperature differences are approximately 9.1 K and 3.6 K for

the exterior south and north with variable exterior surface CHTCs, respectively. Finally, with the increase in plan area densities from $\lambda_p = 0$ (isolated building) to $\lambda_p = 0.44$ (denser cities), the shading effect significantly affected the energy consumption with a 32% increase in the heating energy consumptuion and a 24% decrease in in cooling enegry consumption. This large difference in energy consumption is primarily due to the shading that results in largely varying wall temperture distributions for isolated buildings and urban buildings. Furthrmore, the same increase in the plan area density from 0 to 0.44 also affected the energy consumption due to the wind sheltering effect on CHTCs, with a 3.5% decrease in the heating energy consumption and a 6.7% increase in the cooling energy consumption. It is important to notice that this uses the built-in feature of EnergyPlus and does not consider the effect of the infiltration rate in the analysis.

This paper discusses implications of selecting suitable CHTCs on a calibrated energy model and broader implications of the developed CHTCs for the cubic buildings in other configuration of urban neighborhoods. The results of this study showed that CHTCs become important if the energy simulation model is to be calibrated in accordance with the stringent requirements of ASHRAE Guideline 14-2002. Wind directions, shape of the buildings, height of the buildings, and spacing of the buildings in the urban neighborhood are four important variables that could infleunce the results of this study. A factor of 25% could be added in the Uncertainty Quantification (UQ) of the energy models to account for the influence of the wind direction and building shapes. While streamlined buildings, such as circular and elliptical shapes tend to have lower CTHCs compared to the results of this study, buildings with a higher frontal area, such as rectangular shapes, tend to have higher CTHCs. In general, any irregular urban neighborhood configuration could be simplified into regular and semi-irregular configurations. For any irregular urban neighborhood, customized CFD simulations are required to calculate the CHTCs for the building energy simulations. Further studies are required to consider detailed variation of the building shapes, urban neighborhood configurations, and wind directions. The results of this study have the greatest implications for cities such as Washington DC where the variation of building height is minimal. Overall, this study quantified the importance of carefully choosing the exterior CHTC correlations to simulate building energy consumption, especially taking into account the cooling energy consumption in urban neighborhoods.

Acknowledgements

This study is sponsored by the EFRI-1038264 award from the National Science Foundation (NSF), Division of Emerging Frontiers in Research and Innovation (EFRI-1038264 / EFRI-1452045). Authors would like to thank Brent Griffith from the NREL EnergyPlus developer's team for sharing his valuable experience on the implementation of the CHTCs in the EnergyPlus program. In addition, authors would like to thank Matthew Dahlhausen and Nicholas W. Mattise at the University of Maryland for reviewing the paper.

References

[1] J.A. Palyvos, A survey of wind convection coefficient correlations for building envelope energy systems' modeling, Applied Thermal Engineering 28 (8–9) (2008) 801–808.
[2] J. Liu, J. Srebric, N. Yu, Numerical simulation of convective heat transfer coefficients at the external surfaces of building arrays immersed in a turbulent boundary layer, International Journal of Heat and Mass Transfer 61 (2013) 209–225.
[3] J.D. Spitler, C.O. Pedersen, D.E. Fisher, Interior convective heat transfer in buildings with large ventilative flow rates, ASHRAE Transactions 97 (1) (1991) 505–515.
[4] D.E. Fisher, C.O. Pedersen, Convective heat transfer in building energy and thermal load calculations, ASHRAE Transactions 103 (2) (1997) 137–148.
[5] I. Beausoleil-Morrison, An algorithm for calculating convection coefficients for internal building surfaces for the case of mixed flow in rooms, Energy and Buildings 33 (4) (2001) 351–361.
[6] M. Mirsadeghi, D. Costola, B. Blocken, J.L.M. Hensen, Review of external convective heat transfer coefficient models in building energy simulation programs: implementation and uncertainty, Applied Thermal Engineering 56 (1–2) (2013) 134–151.
[7] J. Liu, M. Heidarinejad, S. Gracik, D. Jareemit, J. Srebric, The impact of surface convective heat transfer coefficients on the simulated building energy consumption and surface temperatures, in: The 13th International Conference on Indoor Air Quality and Climate, Hong Kong, 2014.
[8] M.G. Emmel, M.O. Abadie, N. Mendes, New external convective heat transfer coefficient correlations for isolated low-rise buildings, Energy and Buildings 39 (3) (2007) 335–342.
[9] B. Blocken, T. Defraeye, D. Derome, J. Carmeliet, High-resolution CFD simulations for forced convective heat transfer coefficients at the facade of a low-rise building, Building and Environment 44 (12) (2009) 2396–2412.
[10] T. Defraeye, B. Blocken, J. Carmeliet, CFD analysis of convective heat transfer at the surfaces of a cube immersed in a turbulent boundary layer, International Journal of Heat and Mass Transfer 53 (1–3) (2010) 297–308.
[11] Y.K. Yi, N. Feng, Dynamic integration between building energy simulation (BES) and computational fluid dynamics (CFD) simulation for building exterior surface, Building Simulation 6 (3) (2013) 297–308.
[12] R. Zhang, K.P. Lam, S.C. Yao, Y.J. Zhang, Coupled EnergyPlus and computational fluid dynamics simulation for natural ventilation, Building and Environment 68 (2013) 100–113.
[13] A. Mochida, I.Y.F. Lun, Prediction of wind environment and thermal comfort at pedestrian level in urban area, Journal of Wind Engineering & Industrial Aerodynamics 96 (10–11) (2008) 1498–1527.
[14] Y. Tominaga, A. Mochida, R. Yoshie, H. Kataoka, T. Nozu, M. Yoshikawa, T. Shirasawa, AIJ guidelines for practical applications of CFD to pedestrian wind environment around buildings, Journal of Wind Engineering & Industrial Aerodynamics 96 (10–11) (2008) 1749–1761.
[15] S. Murakami, R. Ooka, A. Mochida, S. Yoshida, S. Kim, CFD analysis of wind climate from human scale to urban scale, Journal of Wind Engineering & Industrial Aerodynamics 81 (1999) 57–81.
[16] Y. Tominaga, A. Mochida, S. Murakami, S. Sawaki, Comparison of various revised k-epsilon models and LES applied to flow around a high-rise building model with 1:1:2 shape placed within the surface boundary layer, Journal of Wind Engineering & Industrial Aerodynamics 96 (4) (2008) 389–411.
[17] M. Kato, B.E. Launder, The modeling of turbulent flow around stationary and vibrating square cylinders, in: Preprints of 9th Symposium on Turbulent Shear Flow, vol. 10(4), 1993, pp. 1–6.
[18] J.T. Shao, J. Liu, J.N. Zhao, Evaluation of various non-linear k-epsilon models for predicting wind flow around an isolated high-rise building within the surface boundary layer, Building and Environment 57 (2012) 145–155.
[19] T. Tamura, Towards practical use of LES in wind engineering, Journal of Wind Engineering & Industrial Aerodynamics 96 (10–11) (2008) 1451–1471.
[20] J. Allegrini, V. Dorer, J. Carmeliet, Analysis of convective heat transfer at building facades in street canyons and its influence on the predictions of space cooling demand in buildings, Journal of Wind Engineering & Industrial Aerodynamics 104 (2012) 464–473.
[21] EnergyPlus Engineering Reference, U.S. Department of Energy, 2012 http://www.energyplus.gov
[22] N. Yaghoobian, J. Kleissl, An indoor–outdoor building energy simulator to study urban modification effects on building energy use–Model description and validation, Energy and Buildings 54 (2012) 407–417.
[23] N.H. Wong, S.K. Jusuf, N.I. Syafii, Y.X. Chen, N. Hajadi, H. Sathyanarayanan, Y.V. Manickavasagam, Evaluation of the impact of the surrounding urban morphology on building energy consumption, Solar Energy 85 (1) (2011) 57–71.
[24] R.W. MacDonald, R.F. Griffiths, D.J. Hall, An improved method for the estimation of surface roughness of obstacle arrays, Atmospheric Environment 32 (11) (1998) 1857–1864.
[25] ANSYS Fluent 12 Theory Guide, ANSYS Inc., US, 2009, April.
[26] E.R. Meinders, T.H. vanderMeer, K. Hanjalic, C.J.M. Lasance, Application of infrared thermography to the evaluation of local convective heat transfer on arrays of cubical protrusions, International Journal of Heat and Fluid Flow 18 (1) (1997) 152–159.
[27] J. Franke, A. Hellsten, H. Schellen, B. Carrissimo, Best Practice Guideline for the CFD Simulation of Flows in the Urban Environment, COST Action 732. Quality Assurance and Improvement of Microscale Meteorological Models, 2007.
[28] A. Hagishima, J. Tanimoto, Field measurements for estimating the convective heat transfer coefficient at building surfaces, Building and Environment 38 (7) (2003) 873–881.
[29] P.J. Richards, R.P. Hoxey, Appropriate boundary-conditions for computational wind engineering models using the kappa-epsilon turbulence model, Journal of Wind Engineering & Industrial Aerodynamics 46 (7) (1993) 145–153.
[30] B. Blocken, J. Carmeliet, High-resolution wind-driven rain measurements on a low-rise building – experimental data for model development and model validation, Journal of Wind Engineering & Industrial Aerodynamics 93 (12) (2005) 905–928.
[31] B. Blocken, T. Stathopoulos, J. Carmeliet, CFD simulation of the atmospheric boundary layer: wall function problems, Atmospheric Environment 41 (2) (2007) 238–252.

[32] S.V. Patankar, Numerical Heat Transfer and Fluid Flow, Hemisphere, Washington, DC, 1980.
[33] R.I. Issa, Solution of the implicitly discretised fluid flow equations by operator-splitting, Journal of Computational Physics 62 (1) (1986) 40–65.
[34] P. Gousseau, B. Blocken, G.J.F. van Heijst, CFD simulation of pollutant dispersion around isolated buildings: on the role of convective and turbulent mass fluxes in the prediction accuracy, Journal of Hazardous Materials 194 (2011) 422–434.
[35] P. Gousseau, B. Blocken, T. Stathopoulos, G.J.F. van Heijst, CFD simulation of near-field pollutant dispersion on a high-resolution grid: a case study by LES and RANS for a building group in downtown Montreal, Atmospheric Environment 45 (2) (2011) 428–438.
[36] F. Mathey, D. Cokljat, J.P. Bertoglio, E. Sergent, Assessment of the vortex method for large Eddy simulation inlet conditions, Progress in Computational Fluid Dynamics 6 (1–3) (2006) 58–67.
[37] ASHRAE Standard 140-2011, Standard Method of Test for the Evaluation of Building Energy Analysis Computer Programs, American Society of Heating, Refrigeration Air Conditioning Engineers Inc., Atlanta, GA, 2011.
[38] ASHRAE, ANSI/ASHRAE Standard 189.1 – 2009: Standard for the Design of High-Performance Green Buildings Except Low-Rise Residential Buildings, ASHRAE, Atlanta, GA, 2009.
[39] M. Deru, K. Field, D. Studer, K. Benne, B. Griffith, P. Torcellini, B. Liu, M. Halverson, D. Winiarski, M. Yazdanian, J. Huang, D. Crawley, U.S. Department of Energy Commercial Reference Building Models of the National Building Stock, NREL, 2011.
[40] G. Han, J. Srebric, E. Enache-Pommer, Different modeling strategies of infiltration rates for an office building to improve accuracy of building energy simulations, Energy and Buildings (2014), http://dx.doi.org/10.1016/j.enbuild.2014.10.028 (Accepted for publication).
[41] ASHRAE Standard 90.1-2007, Energy Standard for Buildings except Low-Rise Residential Buildings, American Society of Heating, Refrigeration Air Conditioning Engineers Inc., Atlanta, GA, 2007.
[42] L.P. Wang, P. Mathew, X.F. Pang, Uncertainties in energy consumption introduced by building operations and weather for a medium-size office building, Energy and Buildings 53 (2012) 152–158.
[43] T. Hong, D. Sartor, P. Mathew, M. Yazdanian, Comparisons of HVAC simulations between EnergyPlus and DOE-2.2 for data centers, ASHRAE Trans. 2009 (2009).
[44] Building Component Library, U.S. Department of Energy, 2012 https://bcl.nrel.gov/
[45] ASHRAE, ASHRAE Handbook – Fundamentals, American Society of Heating, Refrigerating, and Air-Conditioning Engineers Inc., Atlanta, 2005.
[46] C. Booten, N. Kruis, C. Christensen, Identifying and Resolving Issues in EnergyPlus and DOE-2 Window Heat Transfer Calculations, National Renewable Energy Laboratory, Denver, USA, 2012, August.
[47] J.T. Shao, J. Liu, J.N. Zhao, W.W. Zhang, D.X. Sun, Z.P. Fu, A novel method for full-scale measurement of the external convective heat transfer coefficient for building horizontal roof, Energy and Buildings 41 (8) (2009) 840–847.
[48] T.R. Oke, Street design and urban canopy layer climate, Energy and Buildings 11 (1–3) (1988) 103–113.
[49] M. Heidarinejad, Relative Significance of Heat Transfer Processes to Quantify Tradeoffs Between Complexity and Accuracy of Energy Simulations With a Building Energy Use Patterns Classification, The Pennsylvania State University, 2014.
[50] ASHRAE Guideline 14-2002, Measurement of Energy and Demand Savings, ASHRAE, 2002.
[51] C. Ratti, S. Di Sabatin, R. Britter, F.B.S. Caton, Analysis of 3-D urban databases with respect to pollution dispersion for a number of European and American cities, Water, Air, and Soil Pollution: Focus 2 (2002) 459–469.
[52] R.D. Clear, L. Gartland, F.C. Winkelmann, An empirical correlation for the outside convective air-film coefficient for horizontal roofs, Energy and Buildings 35 (8) (2003) 797–811.
[53] S.E.G. Jayamaha, N.E. Wijeysundera, S.K. Chou, Measurement of the heat transfer coefficient for walls, Building and Environment 31 (5) (1996) 399–407.
[54] Y. Sun, L. Gu, C.F.J. Wu, G. Augenbroe, Exploring HVAC system sizing under uncertainty, Energy and Buildings 81 (0) (2014) 243–252.
[55] H. Versteeg, W. Malalasekera, An Introduction to Computational Fluid Dynamics: The Finite Volume Method, 2nd edition, Longman Scientific & Technical, 2007.
[56] E. Solazzo, S. Vardoulakis, X. Cai, A novel methodology for interpreting air quality measurements from urban streets using CFD modelling, Atmospheric Environment 45 (29) (2011) 5230–5239.
[57] P.A. Mirzaei, J. Carmeliet, Dynamical computational fluid dynamics modeling of the stochastic wind for application of urban studies, Building and Environment 70 (0) (2013) 161–170.
[58] E.M. Sparrow, J.P. Abraham, J.C.K. Tong, Archival correlations for average heat transfer coefficients for non-circular and circular cylinders and for spheres in cross-flow, International Journal of Heat and Mass Transfer 47 (24) (2004) 5285–5296.
[59] B.J. Burley, Infiltration Mapping for Urban Environments (PhD dissertation), The Pennsylvania State University, 2009.
[60] J. Liu, J. Srebric, N. Yu, A rapid and reliable numerical simulation method for predictions of outdoor thermal environment in actual urban areas, in: The ASME 2013 Summer Heat Transfer Conference (HT 2013), Minneapolis, MN, 2013.
[61] S. Gracik, The Effect of Urban Density Building HVAC Performance, The Pennsylvania State University, 2014.